JOURNAL OF MATERIALS SCIENCE **39** (2004) 7153–7159

Model based gap and melt rate control for VAR of Ti-6Al-4V

J.J. BEAMAN
Department of Mechanical Engineering, University of Texas, Austin, Texas 78712, USA

R. L. WILLIAMSON, D. K. MELGAARD, G. J. SHELMIDINE
Liquid Metals Processing Laboratory, Sandia National Laboratories, Albuquerque, New Mexico 87185-1134, USA
E-mail: rodwill@sandia.gov

J. C. HAMEL
Timet Corporation, Henderson, Nevada 89009, USA

A new controller has been designed for vacuum arc remelting titanium alloys based on an accurate, low order, nonlinear, melting model. The controller adjusts melting current and electrode drive speed to match estimated gap and melt rate with operator supplied reference values. Estimates of gap and melt rate are obtained by optimally combining predictions from the model with measurements of voltage, current, and electrode position. Controller tests were carried out at Timet Corporation's Henderson Technical Laboratory in Henderson, Nevada. Previous test results were used to correlate measured gap to voltage and current. A controller test melt was performed wherein a 0.279 m diameter Ti-6Al-4V electrode was melted into 0.356 m diameter ingot. Commanded melt rate was varied from 20 to 90 g/s and commanded gap was held at 1.5 cm. Because no measure of electrode weight was available on the test furnace, electrode position data were analyzed and the results used to determine the actual melt rate. A gap-voltage-current factor space model was used to check estimated gap. The controller performed well, and both melt rate and electrode gap control were successfully demonstrated.

1. Introduction

Over the past several years, Sandia National Laboratories and the Specialty Metals Processing Consortium have invested significant resources into improving control of the vacuum arc remelting (VAR) process. Producing high quality VAR ingots with improved yield requires accurate, transient control of melt rate and electrode gap. This is difficult because of the long melt transients induced in a VAR electrode with changing current. One way to achieve melt rate control is to apply a pre-computed, open loop current schedule. Bertram et al. demonstrated this approach while VAR processing an Alloy 718 electrode [1]. However, open loop approaches are not robust with respect to changes in process conditions. Robust feedback control of melt rate (and electrode gap) in the VAR process requires knowledge of the melting conditions through measurements, which are then incorporated into an overall feedback control system.

Besides being unresponsive to changing melting conditions and process disturbances, open loop control requires that the melt schedule be specifically designed ahead of time for each melt rate change required. Therefore, a real solution to the dynamic melt rate problem requires development of a closed loop controller that tracks the thermal conditions in the electrode and calculates the appropriate current response "on the fly." Beaman and coworkers have described such a controller [2]. The controller employs measurements and a low order, nonlinear melting model, to track thermal conditions in the electrode throughout the melt. This method does not require heavily filtered load cell data to obtain a measure of electrode weight for feedback. Indeed, although a measurement of electrode weight is highly desirable for improved performance, it is not necessary.

A linear version of the controller has been applied to VAR of 304 stainless steel [3] as well as Alloy 718 [4]. The linear version works well as long as the melt rate does not change dramatically from its nominal value during the course of melting. However, when required to control through large melt rate ranges, the linear controller shows significant error. A nonlinear version of the controller was developed to alleviate this problem.

This paper reports the implementation and testing of a nonlinear, dynamic VAR process controller that can maintain effective control through a very large range of commanded melt rate. Dynamic, in this case, means that the process variables are changed on a time scale that is short compared to the time required for the thermal distribution in the electrode to reach steady state. This

technology enables melting engineers to easily implement extremely aggressive melt rate schedules while simultaneously maintaining accurate control of electrode gap. Furthermore, it makes this possible on furnaces that are not equipped with load cell transducers to measure electrode weight. The test work described herein was performed on a VAR furnace at Timet Corporation's Henderson Technical Laboratory while melting Ti-6Al-4V. The test furnace is not equipped with load cell transducers to measure electrode weight.

2. Controller structure

The control is designed with a model-based philosophy. It is based on the premise that physical understanding of the process should be combined with measurements to provide an optimal estimate of the quantities to be controlled. Once a good estimate of these quantities is obtained, controlling the system is often straightforward.

The melting dynamics of the electrode can be effectively modeled as a Stefan moving boundary problem [5] using the following equations.

$$\rho(T)C(T)\frac{\partial T}{\partial t} = \frac{\partial}{\partial x}\left(K(T)\frac{\partial T}{\partial x}\right) \quad (1)$$

$$P_{\mathrm{m}}(I,G) + K(T)A_{\mathrm{e}}\left.\frac{\partial T}{\partial x}\right|_{\mathrm{S}} = \rho L^{*}A_{\mathrm{e}}\dot{S} \quad (2)$$

$$V = v_0 + R_{\mathrm{I}}I + R_{\mathrm{G}}GI \quad (3)$$

$$P_{\mathrm{m}} = \mu V I \quad (4)$$

$$L^{*} = \bar{h}_{\mathrm{sup}} - \bar{h}_{\mathrm{m}} \quad (5)$$

$$T(S,t) = T_{\mathrm{m}} \quad (6)$$

$$T(\infty,t) = T_{\mathrm{r}} \quad (7)$$

In these equations, T is temperature, x is distance down the electrode, t is time, P_{m} is melt power on the bottom face of the electrode, I is current, G is electrode gap, ρ is mass density, C is heat capacity, K is thermal conductivity, A_{e} is electrode area, S is burn off length, sup is a subscript for superheat property, m is a subscript for melt property, r is a subscript for room temperature property, L^{*} is the latent heat plus superheat in the melted material, V is voltage, v_0 is the cathode fall voltage, R_I is resistance independent of gap, R_{G} is gap sensitive resistance per length, μ is melt efficiency, and $\bar{h}$ is mass specific enthalpy. The melt efficiency is defined to be the percentage of total electrical power that goes into actually melting the electrode.

As described in Beaman *et al.*[2] these partial differential equations can be approximated as ordinary differential equations describing the dynamics of the melting electrode in terms of two state variables, thermal boundary layer thickness (Δ) and electrode gap (G), and two inputs, current (I) and electrode ram speed (V_{ram}):

$$\dot{\Delta} = \frac{C_{\Delta\Delta}\alpha_{\mathrm{r}}}{\Delta} - \frac{C_{\Delta\mathrm{p}}}{h_{\mathrm{m}}}p_{\mathrm{m}}$$

$$\dot{G} = a\dot{S} - V_{\mathrm{ram}} = a\left(-\frac{\alpha_{\mathrm{r}}C_{\mathrm{S}\Delta}}{\Delta} + \frac{C_{\mathrm{Sp}}}{h_{\mathrm{m}}}p_{\mathrm{m}}\right) - V_{\mathrm{ram}} \quad (8)$$

$\alpha = K/\rho C$ in this equation is thermal diffusivity, and the coefficients, defined as

$$C_{\Delta\Delta} = \frac{224(\Lambda+1)\left(\frac{1}{2}+\frac{\gamma h_{\mathrm{m}}}{3}\right)}{3\Lambda+11}, \quad C_{\Delta\mathrm{p}} = \frac{32\Lambda}{3\Lambda+11}$$

$$C_{\mathrm{S}\Delta} = \frac{56\Lambda\left(\frac{1}{2}+\frac{\gamma h_{\mathrm{m}}}{3}\right)}{3\Lambda+11}, \quad C_{\mathrm{Sp}} = \frac{11\Lambda}{3\Lambda+11} \quad (9)$$

are functions of volume specific melt enthalpy, h_{m}, Stefan number, $\Lambda = \frac{(h_{\mathrm{sup}}-h_{\mathrm{m}})}{h_{\mathrm{m}}}$, and the diffusivity parameter γ that relates enthalpy per volume h to diffusivity according to

$$\alpha = \alpha_{\mathrm{r}}(1+\gamma h). \quad (10)$$

p_m in Equations 8 is the melt power flux, which is a function of current and gap, and a accounts for the difference between electrode area A_{e} and ingot area A_{i}. These variables are described by the following equations:

$$p_{\mathrm{m}} = \mu(v_{\mathrm{o}}I + (R_{\mathrm{I}} + R_{\mathrm{G}}G)I^2)/A_{\mathrm{e}} \quad (11)$$

$$a = 1 - \frac{A_{\mathrm{e}}}{A_{\mathrm{i}}}. \quad (12)$$

Since electrode gap is a state, it can be obtained directly from the solution of the differential equations. Melt rate, on the other hand, is not a state, but it can be expressed as a function of states and inputs as

$$\dot{m} = \rho A_{\mathrm{e}}\dot{S} = \rho A_{\mathrm{e}}\left(-\frac{\alpha_{\mathrm{r}}C_{\mathrm{S}\Delta}}{\Delta} + \frac{C_{\mathrm{Sp}}}{h_{\mathrm{m}}}p_{\mathrm{m}}(I,G)\right). \quad (13)$$

Equations 8 and 13 do a remarkably good job of predicting melt rate and electrode gap. In References 2–4, these equations are linearized about a nominal melt rate and gap, and used to design a VAR controller. This works very well for melt rates and gaps that remain close to the nominal values. However, in some VAR applications there can be large changes in commanded melt rate (or, alternatively, current) between start-up and steady-state melting, and between steady-state melting and the final hold state. In this case, the linearized controller will not give accurate results. Fig. 1 shows simulation results using Equations 8 through 13 with a linearized controller. This is a simulation of a Ti-6Al-4V VAR melt that starts at the nominal melt rate of 465 gm/s, is commanded to ramp up to 500 gm/s in 400 s, hold for 1600 s, and then ramp down to 60 gm/s in 2000 s. Electrode gap has been commanded to remain constant at 6 cm throughout the melt. Electrode diameter is 76.2 cm and ingot diameter is 91.4 cm. As can be seen in Fig. 1, the estimated responses and the actual responses are very close for small changes from nominal, but these responses deviate significantly when there are large changes.

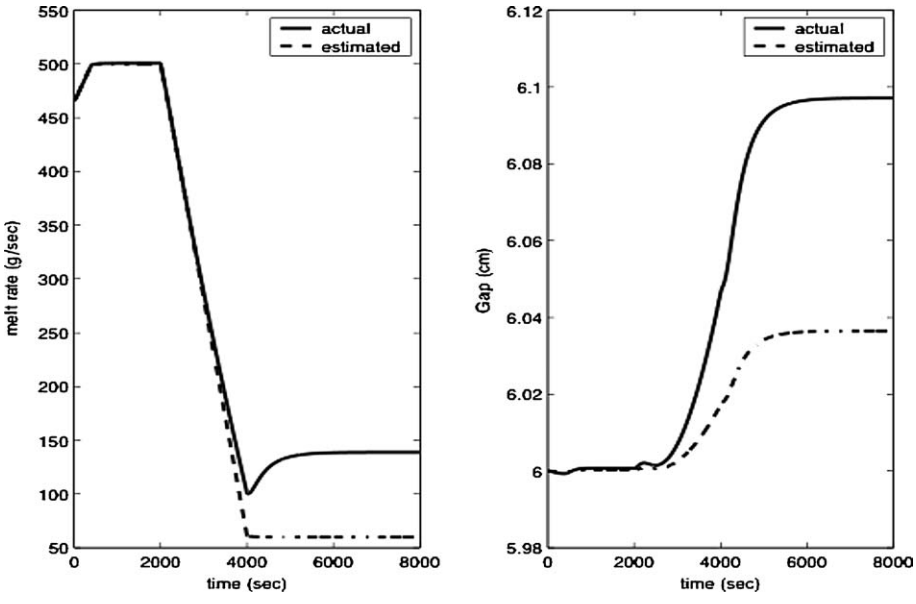

Figure 1 Response of Linear Controller to small and large melt rate commands with nominal melt rate equal to 465 gm/s and nominal gap equal to 6 cm.

2.1. Nonlinear controller

A nonlinear controller was developed to alleviate the problem described above. The essence of the melt rate and electrode gap control problem for a VAR furnace can be stated as follows: given desired values for the outputs $\dot{m}_{\mathrm{d}}$ and G_{d}, determine the time varying current and ram speed commands (I_{C} and $V_{\mathrm{ram_C}}$) required to establish and maintain these outputs. Conceptually, this can be done using Equations 8 through 13. The normal causality for these equations is to input current and ram speed as functions of time and then integrate to obtain electrode gap and thermal boundary layer thickness, and thus melt rate. Control requires inverting this normal causality. For these relatively simple equations, this can be done analytically by first solving Equation 13 for the commanded melt power flux, $p_{\mathrm{m_C}}$. The result is

$$\tilde{p}_{\mathrm{m_C}} = \frac{\dot{m}_{\mathrm{d}} h_{\mathrm{m}}}{\rho A_{\mathrm{e}} C_{\mathrm{Sp}}} + \frac{\alpha_{\mathrm{r}} C_{\mathrm{S}\Delta} h_{\mathrm{m}}}{C_{\mathrm{Sp}} \Delta}. \tag{14}$$

The desired current can then be found by inverting Equation 11:

$$\tilde{I}_{\mathrm{c}} = \frac{-v_0 + \sqrt{v_0^2 + \frac{4\tilde{p}_{\mathrm{m_C}} A_{\mathrm{e}}}{\mu}}}{2(R_{\mathrm{I}} + R_{\mathrm{G}} G)}. \tag{15}$$

Finally, the desired ram speed can be determined from combining Equations 11 and 13 to give

$$\tilde{V}_{\mathrm{ram_C}} = \frac{a\dot{m}_{\mathrm{d}}}{\rho A_{\mathrm{e}}}. \tag{16}$$

There are two problems with directly using 15 and 16 as control laws. First, Equation 15 requires accurate knowledge of G and Δ. There are methods of estimating G from voltage measurements, but there is no direct measurement of Δ. Second, Equation 16 does not guarantee that the actual gap converges to G_{d}. It only ensures that the gap will remain constant if the actual melt rate is equal to $\dot{m}_{\mathrm{d}}$. To solve the first problem, a dynamic estimator can be constructed to estimate Δ and G. The second problem can be solved by adding a correction term to Equation 16 that assures G converges to G_{d}. The control equations then become

$$p_{\mathrm{m_C}} = \frac{\dot{m}_{\mathrm{d}} h_{\mathrm{m}}}{\rho A_{\mathrm{e}} C_{\mathrm{Sp}}} + \frac{\alpha_{\mathrm{r}} C_{\mathrm{S}\Delta} h_{\mathrm{m}}}{C_{\mathrm{Sp}} \hat{\Delta}} \tag{17}$$

$$I_{\mathrm{c}} = \frac{-v_0 + \sqrt{v_0^2 + \frac{4p_{\mathrm{m_C}} A_e}{\mu}}}{2(R_I + R_G \hat{G})} \tag{18}$$

$$V_{\mathrm{ram_C}} = \frac{a\dot{m}_{\mathrm{d}}}{\rho A_{\mathrm{e}}} - K_{\mathrm{G}}(G_{\mathrm{d}} - \hat{G}). \tag{19}$$

where $\hat{}$ stands for an estimated quantity and K_{G} is a feedback gain. This gain is determined by setting it equal to $1/\tau_{\mathrm{G}}$ where τ_{G} is the desired time constant for the gap to reach steady state.

2.2. Nonlinear estimator

Given precise measurements, the control law (17) through (19) above can be designed to give excellent steady state and transient control of both gap and melt rate. At first glance, achieving precise estimation appears to be a daunting task. Gap measurement is inherently noisy and uncertain, and there is no direct measurement of boundary layer thickness, both of which are required to implement the control equations. The key to success is an optimal combination of all available measurements with model predictions. For linear systems, a Kalman filter can do this [6]. Kalman filtering can be extended to nonlinear systems by using a similar form, which consists of a nonlinear state propagation equation to estimate the changes of the state variables, and then combining these estimates with measurements at discrete times. A nonlinear state propagation for a discrete time process can be expressed as

$$\hat{\mathbf{x}}(n+1 \mid n) = \hat{\mathbf{x}}(n \mid n) + \mathbf{f}(\hat{\mathbf{x}}(n \mid n), \mathbf{u}(n))T_{\mathrm{s}} \tag{20}$$

and the measurement update is

$$\hat{\mathbf{x}}(n+1\,|\,n+1) = \hat{\mathbf{x}}(n+1\,|\,n) + \mathbf{M}[\mathbf{z}(n+1) - \mathbf{h}(\hat{\mathbf{x}}(n+1\,|\,n), \mathbf{u}(n)]. \quad (21)$$

where $\hat{\mathbf{x}}$ is a vector of estimated states, $\mathbf{u}(n)$ is a vector of inputs given at time step n, $\mathbf{f}$ is the rate equation obtained from a physical model of the process, and T_s is discrete sample time. The notation $(n+1|\,n)$ denotes an estimated variable at the $n+1$ time step given a measurement at time step n, and $\mathbf{z}(n)$ is a measurement taken at time step n. The measurement vector is related to the state vector and the input vector by

$$\mathbf{z} = \mathbf{h}(\mathbf{x}, \mathbf{u}) \quad (22)$$

where $\mathbf{h}$ is vector function that relates measurements to states and inputs. The matrix $\mathbf{M}$ is a set of estimator gains that are chosen by linearizing the rate function $\mathbf{f}$ and the measurement function $\mathbf{h}$ about nominal values and then using standard Kalman filter theory [6] to obtain the gain matrix $\mathbf{M}$.

There are two primary states, Δ and G. A ram position state (X_{ram}) is added in order to use position as a measurement. To account for variations in melting due to disturbances from steady state, efficiency (μ) is also added as a state. Finally, to account for inaccuracies and bias in current and electrode ram drive inputs, current bias (I_b) and ram speed bias (V_{ram_b}) are added as states. The state vector and input vector for the VAR process used in the present experiment can then be expressed as

$$\mathbf{x} = \begin{bmatrix} \Delta \\ G \\ X_{\text{ram}} \\ \mu \\ I_b \\ V_{\text{ram}_b} \end{bmatrix}, \quad \mathbf{u} = \begin{bmatrix} I_C \\ V_{\text{ram}_C} \end{bmatrix}. \quad (23)$$

The rate function $\mathbf{f}(\hat{\mathbf{x}}, \mathbf{u})$ is given by

$$\mathbf{f}(\hat{\mathbf{x}}, \mathbf{u}) = \begin{bmatrix} \frac{C_{\Delta\Delta}\alpha_r}{\hat{\Delta}} - \frac{C_{\Delta p}}{h_m} p_m(I_C + \hat{I}_b, \hat{G}, \hat{\mu}) \\ a\left(-\frac{\alpha_r C_{S\Delta}}{\hat{\Delta}} + \frac{C_{Sp}}{h_m} p_m(I_C + \hat{I}_b, \hat{G}, \hat{\mu})\right) - (V_{\text{ram}_C} + \hat{V}_{\text{ram}_b}) \\ V_{\text{ram}_C} + \hat{V}_{\text{ram}_b} \\ 0 \\ 0 \\ 0 \end{bmatrix} \quad (24)$$

where total input furnace current is modeled as a commanded term, I_C, plus a bias term, I_b. Total input furnace ram velocity is expressed in a similar manner. The zero rows correspond to efficiency and the two bias states. These terms are modeled as random walk processes to be described below. "Measured" gap is based on a measurement model involving measured voltage (V_m) and current (I_m) as determined by inverting Equation 3:

$$G_m = k_0 + k_1 \frac{1}{V_m} + k_2 \frac{V_m}{I_m} \quad (25)$$

where k_0, k_1, and k_2 are obtained experimentally. The other measurement is ram position, X_m. The measurement vector is then

$$\mathbf{z} = \begin{bmatrix} G_m \\ X_m \\ I_m \end{bmatrix}. \quad (26)$$

A diagram of the controller implementation is shown in Fig. 2. The feedback functions are given by

$$f_G = \frac{a\dot{m}_d}{\rho A_e} \quad (27)$$

$$f_P = \frac{h_m}{C_{Sp}}\left(\frac{\dot{m}_d}{\rho A_e} + \frac{\alpha_r C_{S\Delta}}{\hat{\Delta}}\right) \quad (28)$$

$$\mathbf{f}_I = \frac{\left(-(v_0 + (R_I + R_G\hat{G})(I_C + \hat{I}_b)) + \sqrt{(v_0 + (R_I + R_G\hat{G})(I_C + \hat{I}_b))^2 + 4(R_I + R_G\hat{G})A_e p_{m_C}/\hat{\mu}}\right)}{2(R_I + R_G\hat{G})}. \quad (29)$$

In the diagram, p_{m_C} is the commanded melt power flux. It is calculated using the estimated value of the thermal boundary layer thickness so that it can properly account for electrode melting dynamics. Commanded current is calculated from the melt power using estimated values for electrode gap and melt efficiency. This allows the process to track melt rate upsets. K_G is the feedback gain for electrode gap.

2.3. Process and measurement uncertainty

The elements of the Kalman gain matrix, $\mathbf{M}$, are obtained from the linear version of the process and measurement model. To obtain the numerical elements of this matrix, it is necessary to estimate both the model and measurement uncertainties. Experimental data are used to make these estimates. Specifically, for the process inputs, there is unbiased noise on the input current and ram speed. The standard deviation of this noise is experimentally obtained from current and processed ram position data when commanding constant current and ram speed. The efficiency, current bias, and ram speed bias are treated as random walk processes. A random walk process is one in which the mean of the

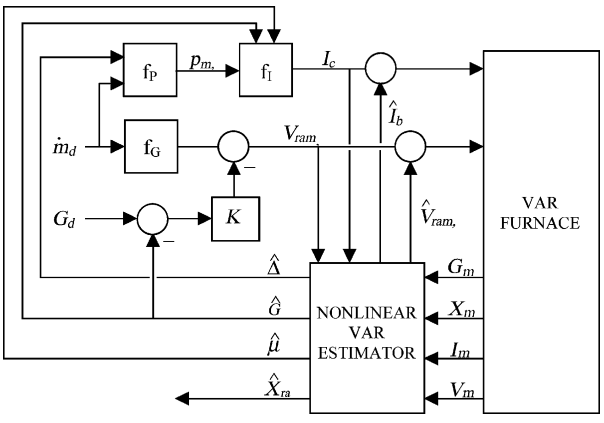

Figure 2 Schematic of the controller layout used on the Timet laboratory VAR furnace.

variable does not change over time (thus the zero coefficients in the rate equation), but its variance increases linearly with time. This means, for example, that the change in efficiency $d\mu$ during time step T_s will have a zero mean but a variance that increases linearly in time as shown below:

$$d\mu = d\beta, \quad \langle d\beta \rangle = 0, \quad \langle d\beta^2 \rangle = \sigma_\mu^2 T_s \qquad (30)$$

where $\langle\rangle$ represents the expectation operator [6]. In this equation, $d\mu$ is the change in efficiency and $d\beta$ is a change in a random walk process (Brownian motion process) with strength σ_μ^2. If $T_s = 1$ second, then the efficiency would be a normal distribution with nominal mean efficiency μ_0 and standard deviation σ_μ. The larger the value of σ_μ the larger the expected time rate of change in efficiency. This value is determined by estimating how fast the efficiency could change due to either a transverse electrode crack, large voids in the electrode, or electrode end effects. Current bias and ram speed bias are also handled as slowly varying random walk processes and have similar noise characteristics to estimate.

Measurements are not perfect and these uncertainties also need to be estimated. The gap measurement is a prime example. Even though drip-short signatures are evident in the voltage output from the Timet laboratory furnace, the controller was designed to estimate electrode gap from voltage and current. A factor space experiment was performed to characterize the relationship. The ranges of current and electrode gap investigated were 4–12 kA and 0.5–5.6 cm, respectively. The following measurement model summarizes the result of this experiment:

$$G_m = -1.071\text{–}1.492 \times 10^5 \frac{1}{I} + 6.159 \times 10^3 \frac{V}{I}. \quad (31)$$

A plot of the measurements against Equation 31 is shown in Fig. 3.

3. Controller data

The experimental data used to design the controller are listed in Tables I and II. Table I contains the process noise and Table II contains measurement uncertainty. A subscripted 0 denotes a nominal value. Nominal values were: $\mu_0 = 0.635$, $a_0 = 0.372$, $I_0 = 10$, 304 A, and $V_{\text{ram}_0} = 8.46 \times 10^{-3}$ cm/s. The thermo-physical properties used for this calculation are listed in Table III. The subscripts r and m stand for room and melt temperature, respectively. Calculations are referenced to room temperature volume specific enthalpy, assigned a value of zero.

TABLE I Process noise levels

Parameter	Noise strength
I	200 A
V_{ram}	1×10^{-3} cm/s
μ	$4 \times 10^{-3} \mu_0$
a	$10^{-2} a_0$
I_b	$10^{-2} / I_0$
V_{ram_b}	$10^{-2} / V_{\text{ram}_0}$

TABLE II Measurement noise

Parameter	Noise strength
G_m	0.33 cm
X_m	0.3 cm
I_m	75 A

TABLE III Thermophysical properties

Parameter	Value
ρ_r	4.46 g cm^{-3}
C_r	0.58 J g^{-1} K^{-1}
K_r	0.069 W cm^{-1} K^{-1}
ρ_m	4.24 g cm^{-3}
C_m	1.14 J g^{-1} K^{-1}
K_m	0.33 W cm^{-1} K^{-1}
L^*	355 J g^{-1}

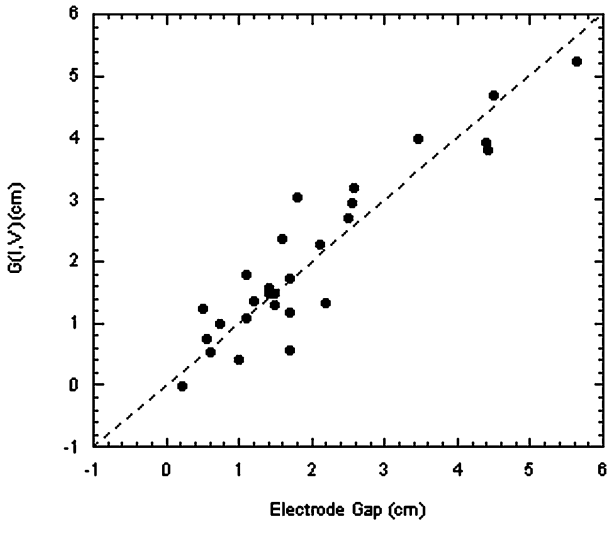

Figure 3 A plot of the gap model as a function of the measured electrode gap.

4. Controller hardware

The controller was implemented on a computer equipped with two PC-MIO-16 I/O cards obtained from National Instruments Corp. (Austin, TX). One card was used to acquire the furnace voltage signal and all other

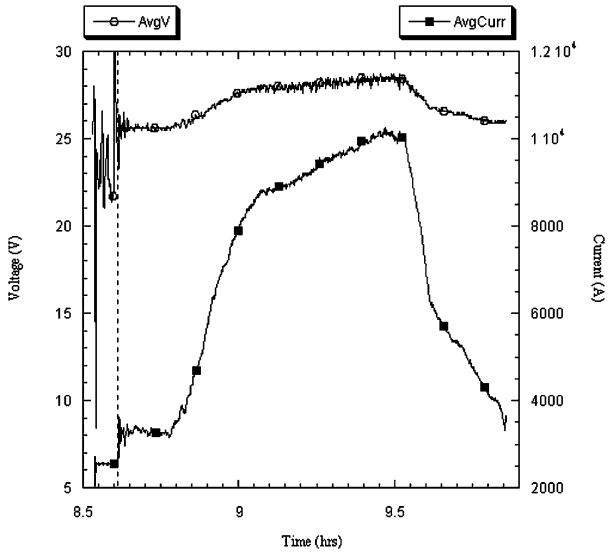

Figure 4 Experimental voltage and current traces with data averaged over 4 s time increments.

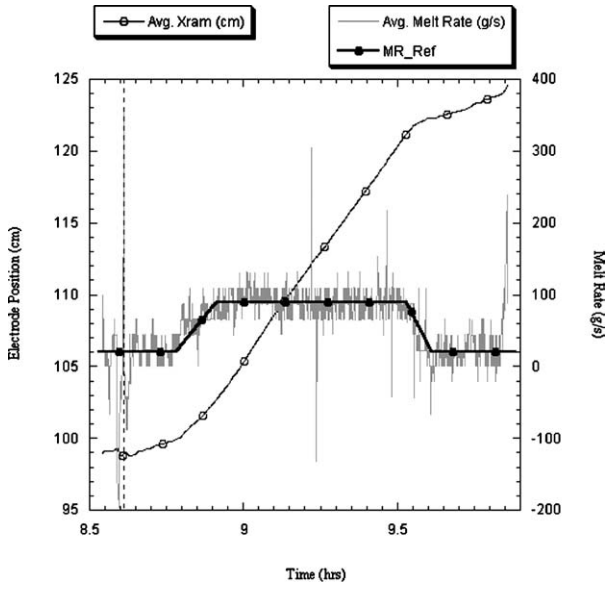

Figure 5 One minute average position and melt rate estimated by differentiating the average position to get V_{ram} and then applying Equation 32.

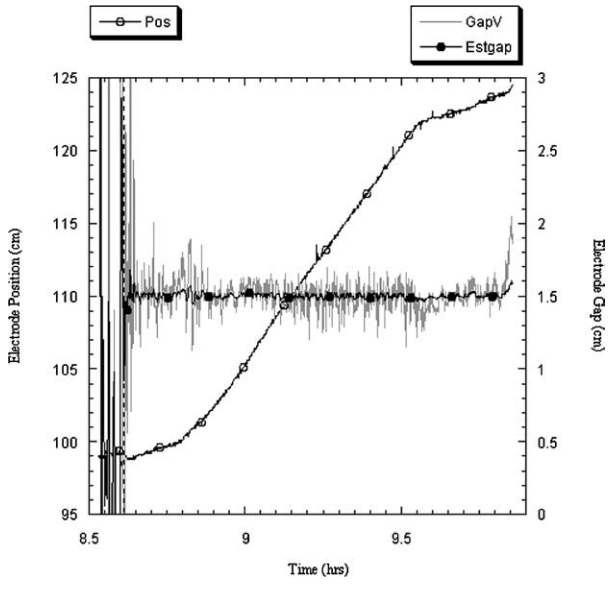

Figure 6 Position and electrode gap traces. GapV in this plot is the gap calculated from the factor space measurement model, Equation 31.

I/O signals were processed with the second card. Signal conditioning was accomplished with isolation amplifiers supplied by Analog Devices (Norwood, MA). A switch was installed to switch control between the new controller and Timet's regular control system. Ram position control was achieved by sending an analog velocity command to an Oilgear (Milwaukee, WI) valve amplifier.

The analog output from a Halmar current transducer (Lem-Dynamp Corp., Grove City, Ohio) and position measuring potentiometer were conditioned and fed into analog input channels of the PC-MIO-16 card. Current control was achieved by supplying a voltage from a D/A port of the card to the power supply control card.

5. Experimental results

An arc was struck using the regular furnace controller and the new controller was switched in as soon as a discernable molten pool had formed. This point may be seen in Fig. 4 where the current trace suddenly jumps from ~2500 to ~3000 A (dashed line). Because this furnace is not equipped with load cell tranducers, the melt rate may not be estimated from electrode mass data. However, melt rate may be related to ram velocity assuming constant electrode gap. The relationship is:

$$\dot{m} = \rho_{\text{m}} A_e V_{\text{ram}} \left(\frac{1}{\chi a} \right) \tag{32}$$

where χ is an experimental correction term for the area ratio parameter found to be ~0.94. If the position data are smoothed for one minute and the result differentiated to obtain V_{ram}, the results of applying Equation 32 to the data are shown in Fig. 5. This results in a relatively noisy melt rate signal but its mean should track close to the actual melt rate. The figure shows that reasonable melt rate control is maintained throughout the melt although some slight overshoot is apparent between ~8.9 and ~9.1 h.

Finally, electrode gap estimated from the measurement model (Equation 31) is plotted in Fig. 6 along with the corresponding reference set point. It is clear that the "measured" gap tracks the reference value of 1.5 cm.

6. Conclusion

The data presented show that the furnace was successfully controlled. Melt rate estimated from position data shows a small overshoot after the initial ramp. Despite this, the fact that this degree of melt rate control was accomplished without load cells for mass feedback is an impressive confirmation of the controller's capability.

Acknowledgment

A portion of this work was supported by the United States Department of Energy under Contract DE-AC04-94AL85000. Sandia is a multiprogram laboratory operated by Sandia Corporation, a Lockheed Martin Company, for the United States Department

of Energy. Support for this work was also provided by the United States Federal Aviation Administration and the Specialty Metals Processing Consortium. The authors gratefully acknowledge the support and cooperation of Titanium Metallurgical Corporation, Henderson, Nevada, for hosting the controller test.

References

1. L. A. BERTRAM, J. BROOKS, D. G. EVANS, A. PATEL, J. A. VAN DEN AVYLE and D. D. WEGMAN, in Proceedings of the 1999 International Symposium On Liquid Metal Processing and Casting, Santa Fe, NM, February 1999, edited by A. Mitchell, L. Ridgeway and M. Baldwin (American Vacuum Society, 1999) p. 156.
2. J. J. BEAMAN, R. L. WILLIAMSON and D. K. MELGAARD, in Proceedings of The 2001 International Symposium On Liquid Metal Processing And Casting, Santa Fe, NM, Sept. 2001, edited by A. Mitchell and J. A. Van Den Avyle (American Vacuum Society, 2001) p. 161.
3. R. L. WILLIAMSON, J. J. BEAMAN, D. K. MELGAARD, G. J. SHELMIDINE, P. K. TUBESING and R. M. AIKIN, Jr., in Proceedings of The 2001 International Symposium On Liquid Metal Processing And Casting, edited by A. Mitchell (American Vacuum Society, 2001) p. 175.
4. R. L. WILLIAMSON, J. J. BEAMAN, D. K. MELGAARD, G. J. SHELMIDINE, A. D. PATEL and C. B. ADASCZIK, in Proceedings of The 2003 International Symposium On Liquid Metal Processing And Casting, edited by Peter Lee, A. Mitchell, J.-P. Bellot and A. Jardy (SF2M, 2003) p. 29.
5. H. CARSLAW and J. JAEGAR, "Conduction of Heat in Solids" (Clarendon Press, Oxford, 1959) Chap. 11.
6. P. S. MAYBECK, "Stochastic Models Estimation and Control" (Academic Press, 1979) Vol. 1.

Received 10 March
and accepted 11 June 2004